LA-UR-08- 7752

*Approved for public release;*
*distribution is unlimited.*

| | |
|---|---|
| *Title:* | Nickel Deficiency in RENi2-xP2 (RE=La, Ce, Pr). Combined Crystallographic and Physical Property Studies |
| *Author(s):* | S. Bobev, S. Xia, E.D. Bauer, F. Ronning, J.D. Thompson, J.L. Sarrao |
| *Intended for:* | Journal of Solid State Chemistry |


Los Alamos National Laboratory, an affirmative action/equal opportunity employer, is operated by the Los Alamos National Security, LLC for the National Nuclear Security Administration of the U.S. Department of Energy under contract DE-AC52-06NA25396. By acceptance of this article, the publisher recognizes that the U.S. Government retains a nonexclusive, royalty-free license to publish or reproduce the published form of this contribution, or to allow others to do so, for U.S. Government purposes. Los Alamos National Laboratory requests that the publisher identify this article as work performed under the auspices of the U.S. Department of Energy. Los Alamos National Laboratory strongly supports academic freedom and a researcher's right to publish; as an institution, however, the Laboratory does not endorse the viewpoint of a publication or guarantee its technical correctness.

Form 836 (7/06)

# Nickel Deficiency in $RENi_{2-x}P_2$ (*RE* = La, Ce, Pr). Combined Crystallographic and Physical Property Studies

*Svilen Bobev and Sheng-qing Xia* [§]

Department of Chemistry and Biochemistry, University of Delaware, Newark, Delaware 19716, U.S.A.

*Eric D. Bauer, Filip Ronning, Joe D. Thompson, and John L. Sarrao*

Materials Physics and Applications Division (MPA-10), Los Alamos National Laboratory, Los Alamos, New Mexico 87545, U.S.A.

**Corresponding author:**

Prof. Svilen Bobev

Department of Chemistry and Biochemistry

University of Delaware

Newark, DE 19716

Phone: (302) 831-8720

Fax: (302) 831-6335

e-mail: *bobev@udel.edu*

**Figure for the graphical abstract:**

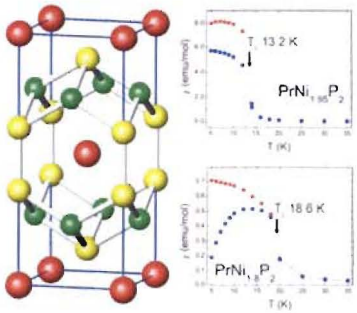


[§] Present address: Dr. Sheng-Qing Xia; State Key Laboratory of Crystal Materials; Institute of Crystal Materials; Shandong University; Jinan, China 250100

# Nickel Deficiency in $RENi_{2-x}P_2$ ($RE$ = La, Ce, Pr). Combined Crystallographic and Physical Property Studies


## Abstract

Large single crystals from $RENi_{2-x}P_2$ ($RE$ = La, Ce, Pr) were synthesized from the pure elements using Sn as a metal flux, and their structures were established by X-ray crystallography. The title compounds were confirmed to crystallize in the body-centered tetragonal $ThCr_2Si_2$ structure type (space group *I*4/*mmm* (No. 139); Pearson's symbol *tI*10), but with a significant stoichiometry breadth with respect to the transition metal. Systematic synthetic work, coupled with accurate structure refinements indicated strong correlation between the degree of Ni-deficiency and the reaction conditions. For four different $PrNi_{2-x}P_2$ ($x \leq 0.5$) samples, temperature dependent *dc* magnetization measurements indicated typical local moment 4*f*-magnetism and a stable $Pr^{3+}$ ground state. Field-dependent heat capacity data confirmed a ferromagnetic order at low temperature, and the variations of $T_C$ with the concentration of Ni defects are discussed. $LaNi_{2-x}P_2$, as expected was found to be Pauli-like paramagnetic in the studied temperature regime, while the Ce-analog $CeNi_{2-x}P_2$ ($x = 0.28(1)$) showed the characteristics of a mixed valent $Ce^{3+}/Ce^{4+}$ system with a possible Kondo temperature on the order of 230 K.



*Keywords*: $PrNi_2P_2$, $CeNi_2P_2$, crystal structure, single-crystal X-ray diffraction, structural disorder.

## 1. Introduction

Ternary intermetallics with the general formula $RM_2X_2$, where $R$ stands for the alkaline-earth and rare-earth metals, $M$ is a transition metal and $X$ denotes an early $p$-block element (groups 13-15), are ubiquitous and frequently investigated [1-30]. Among these, the most commonly encountered structures are the body-centered tetragonal $ThCr_2Si_2$ (Pearson's symbol $tI10$, three-dimensional framework) and the layered trigonal $CaAl_2Si_2$ (Pearson's symbol $hP5$). Both structures are relatively simple and are described by three crystallographically unique sites occupied by the three prototypical elements. Previous theoretical considerations based on the density functional theory (DFT) and the extended Hückel method [5-10] have brought clear understanding of the atomic site preferences, as well as the similarities and the differences between the geometric and electronic requirements in both cases. The two structure types are widely known as very robust and typically present excellent candidates for tuning of particular property of interest by rational substitutions on specific sites (via changes of the electron count, electronegativity and size of the constituent elements). Examples of this approach abound [2,18-25], including several case studies from our laboratory [26-30].

As part of our continuing efforts to better understand the structure-property relationships in Zintl phases and intermetallics, we turned our attention to the chemical bonding and physical properties of various $R_xT_yPn_z$ ternary compounds, where $Pn$ = pnicogen, i.e., group 15 element. These investigations were inspired by the very recent discovery of superconductivity in doped $BaFe_2As_2$ (long known compound with the $ThCr_2Si_2$ type) [22-25] and in a range of oxi-pnictides with the related ZrCuSiAs type [31]. Although, as noted above, a considerable amount of work on ternary pnictides has

already been done, gaps and inconsistencies in the literature are plentiful. For example, the existence of the $RENi_2P_2$ (*RE* = La, Ce, Pr) compounds was first reported in 1980 by Jeitschko *et al.* [32]. They were initially recognized from their X-ray powder diffraction patterns only, but in 1984 [33], the structures of $RENi_2P_2$ (*RE* = La and Ce) were established by single-crystal work. Despite the high-quality crystallography, a basic question regarding the structure remained open in the latter study, namely – the nature of the "small deviations, about 5% from full occupancy of the Ni and P positions" [33]. The authors state that even though the "refined with partial occupancy positions are highly significant from the standpoint of error analysis, it is, however, difficult to assess the physical meaning of this result", and that "the ideal formulas $LaNi_2P_2$ and $CeNi_2P_2$ are well within the homogeneity ranges of the compounds". The herein presented results address this issue and provide a possible explanation as to why non-stoichiometry among the late transition-metal pnictides with the $ThCr_2Si_2$ structure is inherent and more widespread than commonly recognized. Our syntheses and structure refinements, together with the property measurements, suggest a wide phase width in $RENi_{2-x}P_2$ (*RE* = La, Ce, Pr), which is strongly dependent on the reaction conditions. These findings underscore the importance of the careful synthetic and structural work, regardless of the apparent simplicity of the targeted phases.

## 2. Experimental

### *2.1 Synthesis*

Handling of the starting materials (pure La, Ce and Pr from Ames Laboratory, Ni and red P from Alfa, used as received) was carried out inside an argon-filled glove box or under vacuum. In a typical experiment, a mixture of the elements with the desired

stoichiometric ratio (total weight *ca.* 500 mg) was loaded in a 2 $cm^3$ alumina crucible, which was then topped off with 2-2.5 grams Sn (Alfa, shots). This ensures 10-15 fold excess of Sn (with respect to the rare-earth metal) as a flux. The crucible was subsequently enclosed and flame-sealed in an evacuated fused silica ampoule. The mixture was heated in a programmable muffle-furnace from to temperatures 1173-1473 K at rate of 50 to 200°/h, allowed to homogenize for 4-8 h, followed by a slow cooling to 873 K at rates of 3 to 5°/h. The flux was subsequently removed by centrifugation; further details on the procedure can be found elsewhere [34].

Several synthetic details of specific importance to the reaction outcome and ultimately, the physical properties, need to be explicitly mentioned here:

1) Reactions with nominal composition *RE* : Ni : P = 1 : 2 : 2 carried out at lower temperatures (1173-1273 K) yielded $RENi_{2-x}P_2$ (*RE* = La, Ce, Pr) with a modest concentration of Ni defects ($x \approx 0$). The crystals obtained by such reactions were usually very small and often inapt for single-crystal X-ray diffraction studies.

2) Reactions with the same nominal composition, but run at higher temperature (1473 K), yielded $RENi_{2-x}P_2$ (*RE* = La, Ce, Pr) with a higher degree of non-stoichiometry ($x \approx 0.25$). The outcomes of such reactions tended to be larger, plate-like single-crystals, together with small amounts of binary side products – $Ni_2P$, $NiP_2$, $Ni_3Sn_4$, $Sn_3P_4$, etc. [1].

3) Reactions with nominal composition *RE* : Ni : P = 1 : 1 : 2, practically independent of the reaction temperature, afforded the most heavily Ni deficient $RENi_{2-x}P_2$ (*RE* = La, Ce, Pr) products. In these cases, higher reaction temperatures seemed to afford the largest concentration of Ni defects, as evidenced for $PrNi_{2-x}P_2$ ($x = 0.53(1)$), discussed below. The representative products of such reactions were plate-like crystals of the title

compounds (major phase), often heavily agglomerated, and polycrystalline mixtures of various binary phases.

4) Reactions with nominal composition *RE* : Ni : P = 1 : 2 : 2, where Ni was cut from a large rod and not finely divided into smaller pieces yielded $RENi_{2-x}P_2$ (*RE* = La, Ce, Pr) with higher degree of non-stoichiometry. Such observation is not difficult to comprehend – the nucleation and crystal growth strongly depend on the concentration, and apparently, the solubility of Ni in the molten Sn correlates with the particle size.

5) The single-crystals of $RENi_{2-x}P_2$ (*RE* = La, Ce, Pr) are stable in air and diluted solutions of HCl (used to etch and clean the surfaces prior to property measurements) and do not appear to loose their metallic luster over long periods of time.

*2.2 Crystallographic Studies*

X-ray powder diffraction patterns were taken at room temperature on a Rigaku MiniFlex powder diffractometer using monochromatized Cu Kα radiation. Samples were prepared by grinding crystals of $RENi_{2-x}P_2$ (*RE* = La, Ce, Pr) to fine powders, and adding a little bit of elemental Si as an internal standard. Data were acquired in $\theta$–$\theta$ scan modes with steps of 0.05° and rates of 3-5 sec/step. The data analysis was carried out using the JADE 6.5 package [35]. The positions of the peaks and their relative intensities matched well with those calculated from the single-crystal work. The least-squares refined unit cell parameters for all analyzed samples are provided in Table 1.

Single-crystal X-ray diffraction data were collected using a Bruker SMART CCD-based diffractometer (3-cirlce goniometer, Mo Kα source). All data collections were carried at 120 K in batch runs at different ω and ϕ angles. Suitable crystals from the synthesized were selected under a microscope and cut to ca. 0.05-0.07 mm in all

dimensions. Many crystals were tried and checked for singularity before picking the best ones. The typical data-collection involved 0.5°-scans in ω with 10-15 seconds/frame exposure and was carried out using the SMART software [36]. Data integration and global unit cell refinement were done using SAINT, respectively [36]. SADABS was used for semi-empirical absorption correction based on equivalents [37].

In all worked cases, inspections of the systematic absence conditions confirmed the tetragonal body-centered Bravias class, suggesting the $ThCr_2Si_2$ type with space group *I*4/*mmm* (No. 139) [1] as the most likely choice as a model. The structure was subsequently refined to convergence by full matrix least-squares methods on $F^2$ using SHELXL [38]. Site occupation factors were checked by freeing the site occupancy factor of an individual site, while the remaining occupation parameters were kept fixed. This resulted in no statistically significant deviations from unity for the rare-earth metal and the phosphorous sites, but the Ni sites were consistently underoccupied, in some case by more than 25%. Such findings are consistent with earlier work on isotypic nickel phosphides such as $UNi_{2-x}P_2$ [16] and $CaNi_{2-x}P_2$ [39], and confirmed by the EDX analysis and the variations of the unit cell constants (Table 1). Attempts to possibly resolve the disorder by finding larger translation periods and/or lower symmetry groups (*e.g.* $I\bar{4}m2$) were unsuccessful. Further details of the data collection and structure refinements parameters for all four data sets are given in Table 2. In the final refinement cycles, the three atomic positions were refined with anisotropic displacement parameters and freed occupancy for the Ni site. Final positional and equivalent isotropic displacement parameters and important bond distances are listed in Tables 3 and 4, respectively. Additional information in the form of CIF has been deposited with Fachinformationszen-

trum Karlsruhe, 76344 Eggenstein-Leopoldshafen, Germany, (fax: (49) 7247-808-666; e-mail: crysdata@fiz.karlsruhe.de) – depository numbers CSD 420100 ($LaNi_{1.70(1)}P_2$); CSD 420101 ($CeNi_{1.72(1)}P_2$); CSD 420102 ($PrNi_{1.89(1)}P_2$); and CSD 420103 ($PrNi_{1.47(1)}P_2$).

*2.3 EDX Analysis*

To corroborate the structure refinements, particularly for the $PrNi_{1.47(1)}P_2$, where the Ni-deficiency is most pronounced, single crystals from the same batch were subjected to elemental micro-analysis. For the purpose, several plate-like crystals with clean surfaces were mounted onto carbon tape and brought inside the vacuum chamber of a Jeol 7400 F electron microscope. The instrument was equipped with an INCA-Oxford energy-dispersive spectrometer and was operated at 10 μA beam current at 15 kV accelerating potential. Many spots on the crystals' surface were analyzed, giving a ratio of Pr : Ni : P = 1 : 1.36 : 2.25 (atomic %, averaged from more than 10 data points). This ratio confirms the deviation from the ideal stoichiometry and agrees well (within the error of the method) with the composition refined from the single-crystal X-ray diffraction data (Table 2). The analysis did not detect any other elements, besides traces of Sn (flux).

*2.4 Property Measurements*

Field-cooled *dc* magnetization measurements were performed in a Quantum Design MPMS-2 SQUID from 5 to 300 K in an applied magnetic field of 500 Oe. The samples (typically 10-20 mg) were secured in wax-paper, wrapped with a Kapton tape. Raw data were corrected for diamagnetic contribution from the holder and converted to molar magnetic susceptibility (units of emu/mol). Zero field-cooled measurements were performed from 5 to 50 K in an applied magnetic field of 100 Oe. All measurements were repeated for specimens from the same batch in order to ensure reproducibility.

Specific heat $C_p(T)$ data were obtained using the thermal relaxation method on a custom-designed system in the temperature range 1.8 – 100 K. Data were gathered without an external magnetic field and in applied fields of 30 kOe and 90 kOe.

## 3. Results and Discussion

### *3.1 Structure and Bonding*

Formerly known as the line compounds $RENi_2P_2$ [32,33], and reformulated herein as the Ni-deficient $RENi_{2-x}P_2$ (*RE* = La, Ce, Pr), crystallize with the $ThCr_2Si_2$ structure, a ternary variant of the $BaAl_4$ type – one of the most popular structure types among intermetallics [1]. Since this atomic arrangement is not without a precedent, only a brief account of the structure will be given here. For a more detailed description, we refer the reader to several comprehensive treatises on the $BaAl_4$ structure and its variants [2-10]. In the following discussions on the chemical bonding and electronic structure, results from previous investigations on the fully-stoichiometric $RENi_2P_2$ [5-10,32,33] will be used and further developed.

In the structure of $RENi_{2-x}P_2$, the La, Ce, and Pr cations (Wyckoff site 2*a*) are in a body-centered tetragonal arrangement (Figure 1), with separation between them equal to the *a*-cell constant. The Ni atoms (Wyckoff site 4*d*, commonly referred to as a *basal* position) form square nets, which are capped from both sides in an alternating fashion by P (Wyckoff site 4*e*, the *apical* position). This bonding pattern results in two-dimensional slabs, in which, each Ni atom is nearly tetrahedrally coordinated by four P atoms, and each P atom is connected to four basal Ni's in a square pyramidal fashion, as depicted on Figure 1. The P atoms from adjacent layers are close together at P–P distances ranging from 2.31 to 2.43 Å, which strongly correlates with the degree of Ni-deficiency and the

size of the lanthanide metal (Table 4). Along these lines, another important observation, which deserves a special mention here is the fact that higher concentration of vacant Ni sites apparently "disturbs" the equilibrium position of the rare-earth metal, residing at the center of a 18-vertex Fedorov polyhedron. This is clearly represented in Figure 1, where the structures of $PrNi_{1.89(1)}P_2$ and $PrNi_{1.47(1)}P_2$ are represented side-by-side with anisotropic displacement parameters (ADP) – the elongation along the [001] direction of the ADP of the Pr atom in $PrNi_{1.47(1)}P_2$, compared to the normal ADP of the Pr atom in $PrNi_{1.89(1)}P_2$ is immediately seen. Notice that this happens regardless of the largely uniaxial cell contraction (*c*-axis decreases by about 2.5 %) caused by the Ni-defects. A simplistic geometric reasoning might explain this, taking into account the need for effective space-filling and the fact that 2 out of 8 next-nearest Ni atoms are missing.

The P–P distances in all four refined structures are within the range or slightly longer than the expected for a single-bonded pair, while the Ni–Ni contacts are on the order of 2.80 Å (Table 4), much longer than the Ni–Ni distances in elemental Ni, 2.49 Å [1]. This is consistent with the previously developed bonding picture for this structure [5-10], which can be rationalized in terms of multi-center five-center six-electron bonds within the layers and two-center two-electron bonds bridging them along the *c*-axis of the tetragonal unit cell. We draw attention to the fact that these contacts between two layers are a variable geometrical factor (expressed in the *c/a* ratio) and show a remarkable tuneability – as discussed by Mewis [39], the series $CaT_2P_2$ for $T$ = Fe, Co, Ni, Cu shows that the interlayer P–P decreases from 2.71 Å to 2.25 Å as the transition metal moves to the right-hand side in the Periodic Table. Taking this into account, state-of the art band structure calculations by Zheng and Hoffmann [5] for a wide range of $T_2X_2$ frameworks

clearly indicate an electronic effect at play here – the polyanionic sub-structure has an optimal count of 14 valence electrons per formula (*N.B.* only *s* and *p* electrons are considered here), and as *d*-bands get progressively filled on moving from left to right and their energy gets lowered, $\sigma^*_{P-P}$ states are depopulated and the P–P separation, consequently, shortened [5]. More recent DFT studies confirm the earlier interpretation by the Hückel method, and suggest that filling the *p–p* $\sigma$-bonding states at the top of the metal *d*-band should also be accompanied by a weakening of the intralayer Ni–P interactions, since electrons will also fill the *d–p* $\sigma^*$ band [9]. This is exactly what we report in Table 1 – as the Ni-deficiency increases, intralayer bonding weakens (*a* increases) and the interlayer bonding strengthens (*c* decreases).

All of the above is well-known, therefore, it is surprising why the formation of Ni-defects in the discussed rare-earth metal nickel-phosphides has remained an overcast issue for such a long time. Defects at transition metals sites are recognized in a number of isotypic phases with late *d*-metals such as $CaNi_{2-x}P_2$ [39], $CaCu_{2-x}P_2$ [39], $SrCu_{2-x}P_2$ [39], $UNi_{2-x}P_2$ [16], $CePd_{2-x}As_2$ [40], and a whole series of lanthanide-based $RENi_{2-x}Sb_2$, [41], to name just a few. Such non-stoichiometry can be explained qualitatively through bonding considerations, noting that lower nickel, palladium or copper content would probably be favored since the fully stoichiometric $RT_2X_2$ phases would have extra valence electrons [42]. Thus, missing Ni atoms can be viewed as a result of the overall drive to optimize the P–P and Ni–P interactions in the structure – reduced nickel content will not change much the population of the P–P bonding states, however, it will significantly reduce the population of the Ni–P anti-bonding states [43]. Such deficiency on the transition metal sites is also common in the related $ZrCuSi_2$ type intermetallics [1], with

the series $CeT_{1-x}Sb_2$ ($T$ = Ni, Cu, Pd, Ag, Cd) [44-46] and $UT_{1-x}Sb_2$ compounds ($T$ = Fe, Co, Ni, Cu, Ru, Pd, Ag and Au) [47-49] being just a few of the many examples.

*3.2 Properties*

Plots of the temperature dependence of the magnetic susceptibility ($\chi$ = M/H) of four differently synthesized $PrNi_{2-x}P_2$ samples are displayed in Figure 2; the heat capacity of $PrNi_{1.47(1)}P_2$ is shown in Figure 3. As evident from the presented $\chi(T)$ data, the magnetic susceptibility increase markedly below ca. 30 K reaching values of *ca.* 6-8 emu/mol for $PrNi_{1.95}P_2$ and $PrNi_{1.89(1)}P_2$. As the concentration of Ni-defects increases, the maximum susceptibility decreases to about 0.7 emu/mol for $PrNi_{1.80}P_2$, while for $PrNi_{1.47(1)}P_2$, it reaches an order of magnitude lower value of 0.08 emu/mol – the lowest of the four specimens. Above 50 K, the magnetic behavior follows the Curie-Weiss law $\chi = C/(T - \Theta_{CW})$ [50], where $C = N_A\mu_{eff}^2/3k_B$ is the Curie constant and $\Theta_{CW}$ is the paramagnetic Weiss temperature. From the linear fits of the inverse susceptibility (a typical plot is presented in Figure 3 – inset), the effective paramagnetic moments ($\mu_{eff}$) were calculated and tabulated in Table 5. The values in all four cases are consistent with the magnetic behavior expected for trivalent Pr — the free-ion effective moment for $Pr^{3+}$ according to the Hund's rules is 3.58 $\mu_B$ [50].

An inspection of the low temperature magnetization curves for the $PrNi_{2-x}P_2$ samples, measured at very weak applied fields provides evidence for complex behavior. Field and zero-field measurements reveal differences in the magnetic susceptibility, which are indicative of the onset of long-range ferromagnetic order (in the case of $PrNi_{1.47(1)}P_2$, possibly ferrimagnetic – see below). The corresponding Curie temperatures, determined from the mid-point in the jump in $d\chi/dT$, show that the transition temperature

increases with increased Ni-defects. Such variations are not surprising, given that the magnetic order in intermetallics with the $ThCr_2Si_2$ type is known to be very sensitive to the *c/a* ratio [2]. In very simplistic terms, one might consider it as an artefact of the number of electrons in conduction bands. If this reasoning holds true for the discussed $PrNi_{2-x}P_2$ samples, the apparent trend is that higher Ni-deficiency leads to more oxidized samples (Table 1 – *c/a* ratio decreases), thereby, higher Curie temperatures. We also note the fact that susceptibility maximum values change about 100-fold on going from nearly stoichiometric $PrNi_{1.95}P_2$ to a defect-rich $PrNi_{1.47(1)}P_2$, which might suggest the proximity of a (chemical) pressure induced phase transition. Our crystallographic data do not provide an evidence for it, nevertheless, we cannot completely rule out the interplay of locally inequivalent Pr sites and crystalline field (CEF) effects as the origin for this behavior. Another experimental fact that highlights the enlarged importance of CEF effects in more Ni-deficient samples is the slight convex curvature of the $\chi^{-1}(T)$ dependence, shown in Figure 3, and the resultant slightly negative Weiss constant $\Theta_{CW}$.

To further study and confirm the nature of the long-range-ordered magnetic ground state of $PrNi_{1.47(1)}P_2$, heat-capacity measurements were carried out in fields up to 90 kOe. The specific heat $C(T)$ is shown in Figure 3, plotted as $C/T$ vs $T$. An anomaly corresponding to the magnetic transition is clearly seen at $T_C \approx 18$ K. As displayed, the anomaly moves up in temperature with increasing field ($T_C \approx 27$ K at $H = 30$ kOe) and broadens considerably, consistent with ferro/ferrimagnetic order. With the applied field further increased to 90 kOe, the peak broadens and eventually disappears. A nuclear Schottky anomaly due to the $Pr^{3+}$ ions is observed at the lowest temperatures, making estimates of the electronic and phonon contributions to the specific heat difficult.

The magnetizations of two different $LaNi_{2-x}P_2$ samples ($x \approx 0.3$) were measured at an applied field of 100 Oe. The data (not shown) indicate very weak and virtually temperature-independent paramagnetism, consistent with the Pauli-like behavior expected for $La^{3+}$ (closed-shell). There was no superconducting transition down to 5 K.

Plots of the magnetic susceptibility and the inverse susceptibility of $CeNi_{1.72(1)}P_2$ as a function of the temperature are displayed in Figure 4. From the $\chi(T)$ and $\chi^{-1}(T)$ dependence, it is clear that the magnetic susceptibility does not follow the Curie-Weiss law. Similar findings were mentioned by Jeitschko and Reehuis for a reportedly stoichiometric $CeNi_2P_2$ [51]. To verify the lack of a typical $Ce^{3+}$ local-moment magnetism in this case, another batch, likely having much less Ni-defects (Table 1) was also measured. The data (not shown) revealed similar behavior in the high-temperature regime and a possible antiferromagnetic ordering transition around 10 K. The latter could not be established reliably due to a small amount impurity phase in the polycrystalline specimen. Nonetheless, both data sets exhibit the characteristics of a mixed valent $Ce^{3+}/Ce^{4+}$ system, one having a possible Kondo temperature on the order of 230 K. Currently, attempts to grow larger single crystals of more Ni-deficient $CeNi_{2-x}P_2$ samples and studying their properties are under way.

## 4. Conclusions

With the present work, the previously known as the line compounds $RENi_2P_2$ (*RE* = La, Ce, Pr) was reexamined. Based on structure refinements and data from property measurements, the title compounds were thereby reformulated as non-stoichiometric, Ni-deficient $RENi_{2-x}P_2$ phases, whose structure accommodates a wide range of defects on the transition metal site. This study also proved a strong dependence of the between the

phase width on the reaction temperatures. The small changes in the Ni-underoccupancy were shown to ultimately affect the magnetism of the synthesized materials, emphasizing once again the importance of the diligence and care in synthesis and structural characterization for understanding the properties of a given material.

**Acknowledgments**

Svilen Bobev gratefully acknowledges funding from the University of Delaware through start-up funds. Work at LANL was performed under the auspices of the U.S. DOE, Office of Science. The authors also thank Mr. Bayrammurad Saparov for his assistance with the SQUID measurements.

**References**

[1] P. Villars, L.D. Calvert (Eds.), Pearson's Handbook of Crystallographic Data for Intermetallic Compounds, 2nd Ed., American Society for Metals, Materials Park, OH, USA 1991, and the desktop edition 1997.

[2] A. Szytula, J. Leciejewicz, in Handbook of Crystal Structures and Magnetic Properties of Rare Earth Intermetallics; CRC Press, Boca Raton, FL, 1994.

[3] E. Parthé, B. Chabot, H.F. Braun, N. Engel. Acta Crystallogr. B39 (1983), 588.

[4] W.B. Pearson, J. Solid State Chem. 56 (1985) 278.

[5] R. Hoffmann, C. Zheng, J. Phys. Chem. 89 (1985) 4175.

[6] C. Zheng, R. Hoffmann, R. Nesper, H.-G. von Schnering, J. Am. Chem. Soc. 108 (1986) 1876.

[7] C. Zheng, R. Hoffmann, J. Solid State Chem. 72 (1988) 58.

[8] J.K. Burdett, G.J. Miller, Chem. Mater. 2 (1990) 12.

[9] D. Johrendt, C. Felser, O. Jepsen, O.K. Andersen, A. Mewis, J. Rouxel, J. Solid State Chem. 130 (1997) 254.

[10] U. Haussermann, S. Amerioun, L. Eriksson, C.-S. Lee, G.J. Miller, J. Am. Chem. Soc. 124 (2001) 4371.

[11] F. Steglich, J. Aarts, C.D. Bredl, W. Lieke, D. Meschede, W. Franz, H. Schäfer, Phys. Rev. Lett. 43 (1979) 1892.

[12] I. Felner, I. Nowik, Solid State Commun. 47 (1983), 831.

[13] C. Broholm, J. K. Kjems, W.J.L. Buyers, P. Matthewes, T.T.M. Palstra, A.A. Menovsky, J.A. Mydosh, Phys. Rev. Lett. 58 (1987) 1467.

[14] W. Jeitschko, R. Glaum, L. Boonk, J. Solid State Chem. 69 (1987) 93.

[15] R. Marchand, W. Jeitschko, J. Solid State Chem. 24 (1978) 351.

[16] T. Ebel, W. Jeitschko, J. Solid State Chem. 116 (1995) 307.

[17] P.G. Pagliuso, J.L. Sarrao, J.D. Thompson, M.F. Hundley, M.S. Sercheli, R.R. Urbano, C. Rettori, Z. Fisk, S.B. Oseroff, Phys. Rev. B 63 (2001) 092406.

[18] I. Nowik, I. Felner, C. Mermelstein, E.R. Bauminger, Hyperfine Interact. 54 (1990) 847.

[19] B. Li, J.D. Corbett Inorg. Chem. 46 (2007) 8812.

[20] F. Ahmadpour, T. Kolodiazhnyi, Y. Mozharivskyj, J. Solid State Chem. 180 (2007) 2420.

[21] A.V. Tkachuk, A. Mar, J. Solid State Chem. 180 (2007) 2298.

[22] A.S. Sefat, R. Jin, M.A. McGuire, B.C. Sales, D.J. Singh, D. Mandrus, Phys. Rev. Lett. 101 (2008) 117004.

[23] N. Ni, S.L. Bud'ko, A. Kreyssig, S. Nandi, G.E. Rustan, A.I. Goldman, S. Gupta, J.D. Corbett, A. Kracher, P.C. Canfield, Phys. Rev. B 79 (2008) 14507.

[24] M. Rotter, M. Tegel, D. Johrendt, I. Schellenberg, W. Hermes, R. Pöttgen, Phys. Rev. B 78 (2008) 020503(R).

[25] M. Rotter, M. Tegel, D. Johrendt, Angew. Chem. Int. Ed. 47 (2008) 7949.

[26] S. Bobev, E.D. Bauer, J.D. Thompson, J.L. Sarrao, J. Magn. Magn. Mater. 277 (2004) 236.

[27] S.Q. Xia, P. King, S. Bobev, Acta Cryst. E62 (2006) i184.

[28] P.H. Tobash, S. Bobev, J. Alloys Compd. 418 (2006) 58.

[29] S. Bobev, J. Merz, A. Lima, V. Fritsch, J.D. Thompson, J.L. Sarrao, M. Gillessen, R. Dronskowski, Inorg. Chem. 45 (2006) 4047.

[30] S-Q. Xia, C. Myers, and S. Bobev, Eur. J. Inorg. Chem. (2008) 4262.

[31] Y. Kamihara, T. Watanabe, M. Hirano, H. Hosono, J. Am. Chem. Soc. 130 (2008) 3296.

[32] W. Jeitschko, B. Jaberg, J. Solid State Chem. 35 (1980) 312.

[33] W.K. Hofmann, W. Jeitschko, J. Solid State Chem. 51 (1984) 152.

[34] M.G. Kanatzidis, R. Pöttgen, W. Jeitschko, Angew. Chem., Int. Ed. 44 (2005) 6996.

[35] JADE Version 6.5, Materials Data, Inc., Livermore, CA 2003.

[36] Bruker *SMART* and *SAINT*, Bruker AXS Inc., Madison, Wisconsin, USA, 2002.

[37] G.M. Sheldrick *SADABS*, University of Göttingen, Germany, 2003.

[38] G.M. Sheldrick *SHELXTL*, University of Göttingen, Germany, 2001.

[39] A. Mewis, Z. Naturforsch., B 354 (1980) 141.

[40] P. Quebe, W. Jeitschko, J. Solid State Chem. 115 (1995) 37.

[41] W.K. Hofmann, W. Jeitschko, J. Less-Common Met. 138 (1988) 313.

[42] For the discussed nickel-phosphides, if stoichiometric, this means a zero formal charge on the $[Ni_2P_2]^0$ framework, i.e., $RENi_2P_2$ will be electron-rich assuming a nominally trivalent *RE* cation.

[43] Along the same line of thinking, it is easy to explain why the vast majority of compounds in this family are transition-metal silicides and germandides with the alkaline-earth and rare-earth cations – they are formally 14 and 15 electron species, respectively, and they are defect-free.

[44] Y. Muro, N. Takeda, M. Ishikawa, J. Alloys Compd. 257 (1997) 23.

[45] A.V. Tkachuk, A. Mar, Acta Crystallogr. E60 (2004) i82.

[46] P.H. Tobash, S. Bobev, Acta Crystallogr. E61 (2005) i174.

[47] D. Kaczorowski, R. Kruk, J.P. Sanchez, B. Malaman, F. Wastin, Phys. Rev. B, 58 (1998) 9227.

[48] S. Bobev, D.J. Mixson, E.D. Bauer, J.L. Sarrao, Acta Crystallogr. E62 (2006) i64.

[49] S. Bobev, D.J. Mixson, E.D. Bauer, J.L. Sarrao, Acta Crystallogr. E62 (2006) i66.

[50] J.S. Smart, Effective Field Theories of Magnetism; Saunders, Philadelphia, PA, 1966.

[51] W. Jeitschko, M. Reehuis. J. Phys. Chem. Solids 48 (1987) 667.

## Figure Captions

**Figure 1.** Representations of the body-centered tetragonal structure of $PrNi_{1.89(1)}P_2$ and $PrNi_{1.47(1)}P_2$ ($ThCr_2Si_2$ type), viewed approximately along the [100] direction. The Ni–P polyanionic framework is emphasized; non-bonding Ni–Ni interactions are shown with open bonds. Anisotropic displacement parameters are drawn at the 95% probability level: Pr atoms are shown with full thermal ellipsoids, Ni atoms are represented with crossed ellipsoids and the P atoms are depicted with open circles. Unit cell is outlined. Online color: Pr – blue, Ni – green, P – red.

**Figure 2.** Main panels: zero field-cooled magnetic susceptibility ($\chi$) versus temperature of four different $PrNi_{2-x}P_2$ samples. Data are gathered at 500 Oe and normalized per mol. The inset shows magnified views at low temperature of the field (red) and zero field-cooled (blue) magnetic susceptibility ($\chi$) versus temperature. Data in this case are gathered at 100 Oe. Italicized formulas represent refined compositions; the remaining ones are estimated from cell volume interpolations – see Table 1.

**Figure 3.** Main panel: Specific heat of $PrNi_{1.47(1)}P_2$ versus temperature without an applied field and at fields of 30 kOe and 9 kOe, respectively. Data are represented in the form $C_p(T)/T$ to clearly show the anomalies due to the magnetic ordering transitions. The inset shows the temperature dependence of the inverse magnetic susceptibility with $T_C$ indicated by an arrow.

**Figure 4.** Main panel: zero field-cooled magnetic susceptibility ($\chi$) versus temperature of two different $CeNi_{2-x}P_2$ ($x = 0.28(1)$). Data are gathered at 500 Oe and normalized per mol. The inset shows the inverse magnetic susceptibility as a function temperature and the line is a fit of a Curie-Weiss law to the data.

**Table 1.** Unit cell constants for the ternary $RENi_{1-x}P_2$ ($RE$ = La, Ce, Pr) compounds, synthesized using different conditions. Data from previous studies are italicized. Cell parameters from this work were determined by powder X-ray diffraction with Si as an internal standard (Cu Kα, room temperature).

| **Compound** | **Unit cell parameters** | | | | **Reference** | **Synthesis method** |
|---|---|---|---|---|---|---|
| ($ThCr_2Si_2$ type) | $a$ /Å | $c$ /Å | $c/a$ | $V$ /Å$^3$ | | |
| *$LaNi_2P_2$* | *4.007(2)* | *9.632(6)* | *2.404* | *154.6* | *[32]* | *770°C - Sn flux* |
| *$LaNi_2P_2$* [a] | *4.010(1)* | *9.604(2)* | *2.395* | *154.4* | *[33]* | *900°C - Sn flux* |
| $LaNi_{1.70(1)}P_2$ [b] | 4.018(2) | 9.485(6) | 2.361 | 153.1 | this work | 1150°C - Sn flux |
| $LaNi_{1.6}P_2$ [c] | 4.023(2) | 9.375(8) | 2.330 | 151.7 | this work | 1150°C - Sn flux, Ni def. |
| *$CeNi_2P_2$* | *3.955(2)* | *9.505(6)* | *2.403* | *148.7* | *[32]* | *770°C - Sn flux* |
| *$CeNi_2P_2$* [a] | *3.958(1)* | *9.489(2)* | *2.397* | *148.7* | *[33]* | *900°C - Sn flux* |
| $CeNi_{1.9}P_2$ [c] | 3.956(2) | 9.489(3) | 2.398 | 148.5 | this work | 900°C - Sn flux |
| $CeNi_{1.72(1)}P_2$ [b] | 3.960(1) | 9.416(1) | 2.377 | 147.6 | this work | 1150°C - Sn flux |
| *$PrNi_2P_2$* | *3.952(2)* | *9.493(6)* | *2.402* | *148.3* | *[32]* | *770°C - Sn flux* |
| $PrNi_{1.95}P_2$ [c] | 3.956(2) | 9.489(6) | 2.399 | 148.5 | this work | 900°C - Sn flux |
| $PrNi_{1.89(1)}P_2$ [b] | 3.959(1) | 9.486(3) | 2.395 | 148.7 | this work | 1000°C - Sn flux |
| $PrNi_{1.8}P_2$ [c] | 3.959(2) | 9.398(5) | 2.374 | 147.3 | this work | 1000°C - Sn flux, Ni def. |
| $PrNi_{1.47(1)}P_2$ [b] | 3.968(1) | 9.269(1) | 2.336 | 145.9 | this work | 1150°C - Sn flux, Ni def. |

[a] Single-crystal refinements reportedly indicate small deviations, *ca.* 5%, from full occupancy on both the Ni and P positions.

[b] Nickel deficiency determined from single-crystal refinements – Table 2.

[c] Composition estimated from Vegard's Law.

**Table 2.** Selected single-crystal data collection and structure refinement parameters for $RENi_{2-x}P_2$ (*RE* = La, Ce, Pr).

| Empirical formula | $LaNi_{1.70(1)}P_2$ | $CeNi_{1.72(1)}P_2$ | $PrNi_{1.89(1)}P_2$ | $PrNi_{1.47(1)}P_2$ |
|---|---|---|---|---|
| Formula weight, $Z = 2$ | 300.66 | 304.8 | 315.57 | 289.15 |
| Crystal system | Tetragonal | | | |
| Space group | *I*4/*mmm*, No. 139 | | | |
| Temperature | 120 K | | | |
| Unit cell dimensions [Å] | $a = 4.0175(4)$ | $a = 3.9440(2)$ | $a = 3.9531(4)$ | $a = 3.9599(8)$ |
| | $c = 9.454(2)$ | $c = 9.3737(10)$ | $c = 9.462(2)$ | $c = 9.246(4)$ |
| Volume [Å$^3$] | 152.59(4) | 145.81(2) | 147.87(4) | 144.98(7) |
| Density [calculated, g/cm$^3$] | 6.544 | 6.942 | 7.088 | 6.624 |
| Radiation | Mo K$\alpha$ , $\lambda = 0.71073$ Å | | | |
| Absorption coefficient [cm$^{-1}$] | 248.9 | 273.2 | 290.7 | 268.1 |
| Reflections collected /unique | 793/76 ($R_{int}$= 0.0254) | 1027/76 ($R_{int}$= 0.0377) | 702/76 ($R_{int}$= 0.0233) | 518/76 ($R_{int}$= 0.0291) |
| Data / restraints / parameters | 76 / 0 / 10 | | | |
| R* indices [$I > 2\sigma_I$] | R1 = 0.0154 | R1 = 0.0188 | R1 = 0.0115 | R1 = 0.0273 |
| | wR2 = 0.0328 | wR2 = 0.0424 | wR2 = 0.0256 | wR2 = 0.0584 |
| R* indices [all data] | R1 = 0.0173 | R1 = 0.0188 | R1 = 0.0118 | R1 = 0.0302 |
| | wR2 = 0.0334 | wR2 = 0.0424 | wR2 = 0.0257 | wR2 = 0.0591 |
| Goodness-of-fit on $F^2$ | 1.218 | 1.164 | 1.111 | 1.210 |
| Largest diff. peak/hole [e/Å$^3$] | 1.456 / –0.692 | 1.121 / –1.117 | 0.542 / –0.438 | 1.242 / –1.037 |

* $R1 = \sum||F_o| - |F_c||/\sum|F_o|$; $wR2 = [\sum[w(F_o^2 - F_c^2)^2]/\sum[w(F_o^2)^2]]^{1/2}$, where $w = 1/[\sigma^2F_o^2 + (A\cdot P)^2 + B\cdot P]$, and $P = (F_o^2 + 2F_c^2)/3$; A and B – weight coefficients.

**Table 3.** Refined atomic coordinates and equivalent isotropic displacement parameters for $RENi_{2-x}P_2$ ($RE$ = La, Ce, Pr).

| Atom | Wyckoff site | $x$ | $y$ | $z$ | $U_{eq}$ (Å$^2$) | Occup. |
|---|---|---|---|---|---|---|
| | | | $LaNi_{1.70(1)}P_2$ | | | |
| La | 2*a* | 0 | 0 | 0 | 0.013(1) | 1.00 |
| Ni | 4*d* | 0 | 1/2 | 1/4 | 0.010(1) | 0.853(6) |
| P | 4*e* | 0 | 0 | 0.3716(2) | 0.009(1) | 1.00 |
| | | | $CeNi_{1.72(1)}P_2$ | | | |
| Ce | 2*a* | 0 | 0 | 0 | 0.009(1) | 1.00 |
| Ni | 4*d* | 0 | 1/2 | 1/4 | 0.008(1) | 0.861(4) |
| P | 4*e* | 0 | 0 | 0.3742(2) | 0.008(1) | 1.00 |
| | | | $PrNi_{1.89(1)}P_2$ | | | |
| Pr | 2*a* | 0 | 0 | 0 | 0.008(1) | 1.00 |
| Ni | 4*d* | 0 | 1/2 | 1/4 | 0.008(1) | 0.946(4) |
| P | 4*e* | 0 | 0 | 0.3737(2) | 0.008(1) | 1.00 |
| | | | $PrNi_{1.47(1)}P_2$ | | | |
| Pr | 2*a* | 0 | 0 | 0 | 0.017(1) | 1.00 |
| Ni | 4*d* | 0 | 1/2 | 1/4 | 0.009(1) | 0.735(7) |
| P | 4*e* | 0 | 0 | 0.3752(3) | 0.008(1) | 1.00 |

**Table 4.** Selected bond distances (in Å) for $RENi_{2-x}P_2$ (*RE* = La, Ce, Pr).

| $LaNi_{1.70(1)}P_2$ | | $CeNi_{1.72(1)}P_2$ | | $PrNi_{1.89(1)}P_2$ | | $PrNi_{1.47(1)}P_2$ | |
|---|---|---|---|---|---|---|---|
| Ni–P | 2.314(1) × 4 | Ni–P | 2.2899(8) × 4 | Ni–P | 2.2973(8) × 4 | Ni–P | 2.293(2) × 4 |
| Ni–Ni | 2.841(1) × 4 | Ni–Ni | 2.7888(1) × 4 | Ni–Ni | 2.7953(3) × 4 | Ni–Ni | 2.8001(1) × 4 |
| P–P | 2.428(5) | P–P | 2.359(3) | P–P | 2.390(3) | P–P | 2.309(8) |
| La–P | 3.089(1) × 8 | Ce–P | 3.0280(6) × 8 | Pr–P | 3.0399(7) × 8 | Pr–P | 3.029(2) × 8 |
| La–Ni | 3.1018(4) × 4 | Ce–Ni | 3.0627(2) × 4 | Pr–Ni | 3.0826(4) × 4 | Pr–Ni | 3.0435(7) × 4 |
| La–La | 4.0175(4) × 4 | Ce–Ce | 3.9440(2) × 4 | Pr–Pr | 3.9531(4) × 4 | Pr–Pr | 3.9599(8)× 4 |

**Table 5.** Effective magnetic moments and ordering temperatures of $RENi_{2-x}P_2$ ($RE$ = La, Ce, Pr). Results from previous studies are italicized.

| Compound | Magnetic order [a] | $\mu_{eff}$ [$\mu_B$] [b] | $\theta_p$ [K] | $T_C$ [K] | Reference | Comment |
|---|---|---|---|---|---|---|
| *$LaNi_2P_2$* | *none* | *Pauli paramagnetic* | | | *[51]* | |
| $LaNi_{1.70(1)}P_2$ | none | Pauli paramagnetic | | | this work | No SC down to 5 K |
| *$CeNi_2P_2$* | *none* | *No Curie-Weiss behavior* | | | *[51]* | |
| $CeNi_{1.72(1)}P_2$ | none | No Curie-Weiss behavior up to 300 K | | | this work | Kondo-like behavior |
| $CeNi_{1.9}P_2$ | unknown | Pauli paramagnetic above 50 K | | | this work | two steps in $\chi$(T) |
| *$PrNi_2P_2$* | *FM* | *3.4* | *12* | | *[51]* | *$T_C$ not reported* |
| $PrNi_{1.95}P_2$ | FM | 3.65 | 1.5 | 13.2 | this work | $T_C$ from $d\chi(T)/dT$ |
| $PrNi_{1.89(1)}P_2$ | FM | 3.59 | 3 | 13.5 | this work | $T_C$ from $d\chi(T)/dT$ |
| $PrNi_{1.8}P_2$ | FM | 3.75 | –22 | 18.6 | this work | $T_C$ from $d\chi(T)/dT$ |
| $PrNi_{1.47(1)}P_2$ | FM/FFM | 3.50 | –36 | 18 | this work | possible FFM |

[a] FM, FFM denote ferro- and ferrimagnetic interactions, respectively.

[b] Effective moments for free ion $Ce^{3+}$ ($4f^1$) and $Pr^{3+}$ ($4f^2$), according to the Hund's rules are 2.54 $\mu_B$ and 3.58 $\mu_B$, respectively.

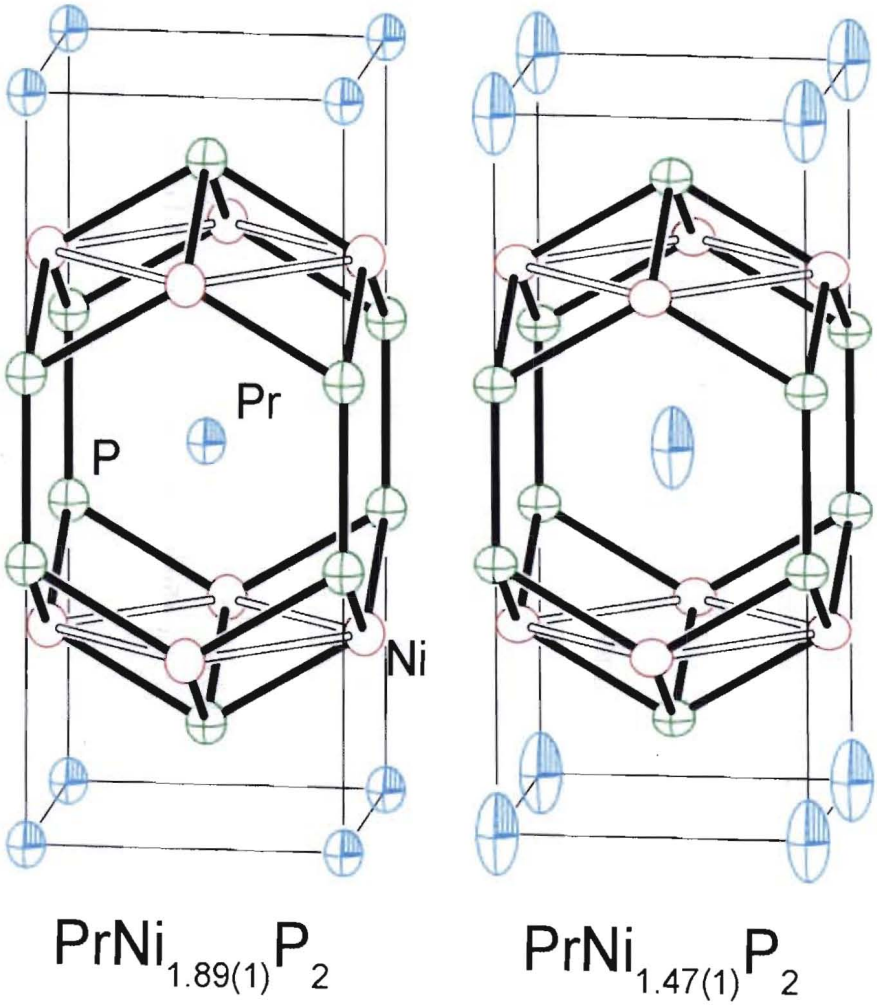


Figure 1.

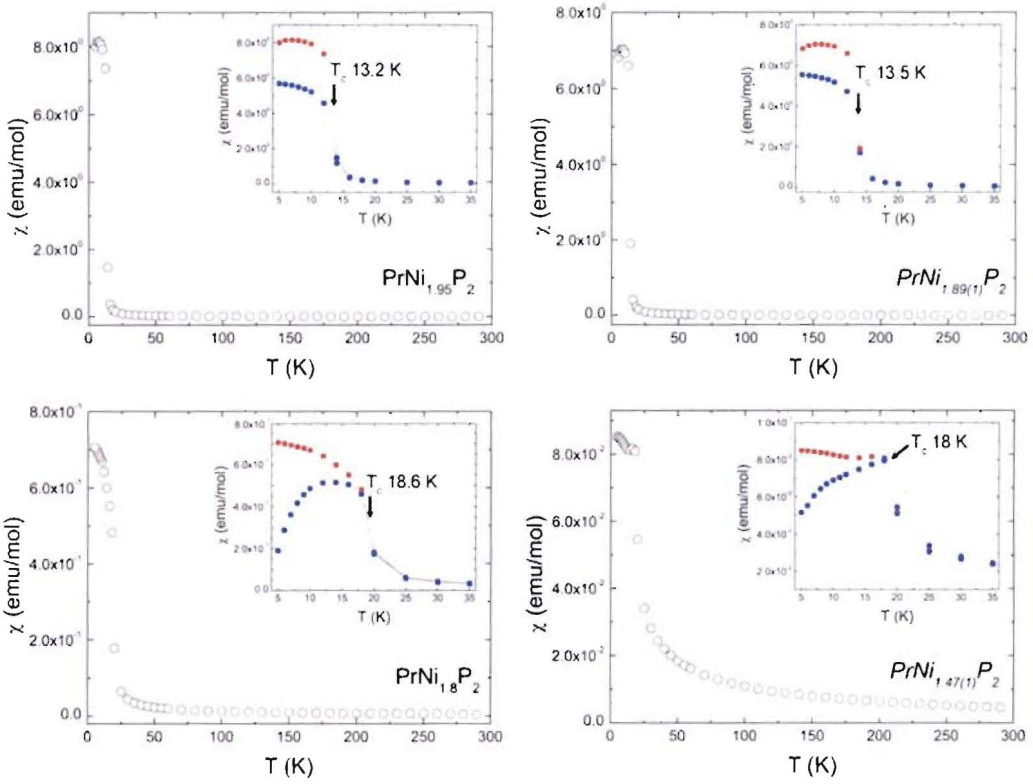
χ (emu/mol)
T (K)
T_c 13.2 K
PrNi1.95P2
T_c 13.5 K
PrNi1.89(1)P2
T_c 18.6 K
PrNi1.8P2
T_c 18 K
PrNi1.47(1)P2

Figure 2.

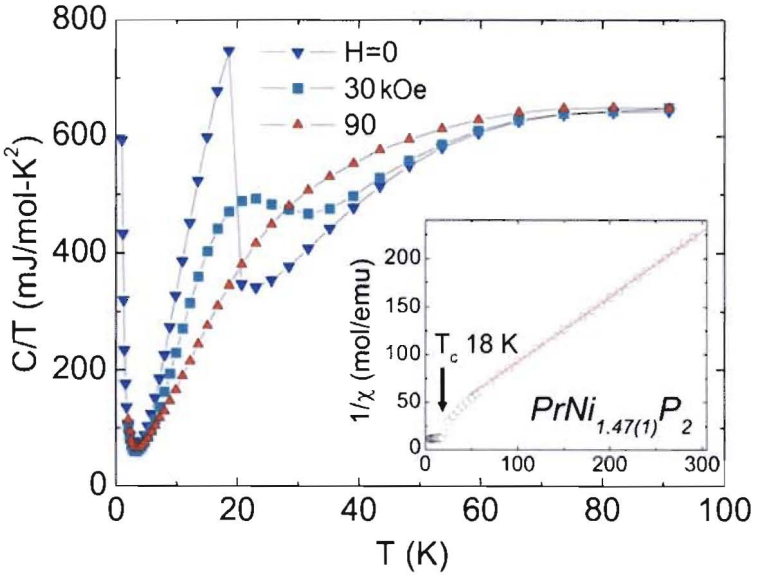
800
600
400
200
0
0
20
40
60
80
100
T (K)
C/T (mJ/mol-K$^2$)
H=0
30 kOe
90
200
150
100
50
0
0
100
200
300
1/χ (mol/emu)
T$_c$ 18 K
PrNi$_{1.47(1)}$P$_2$

Figure 3.

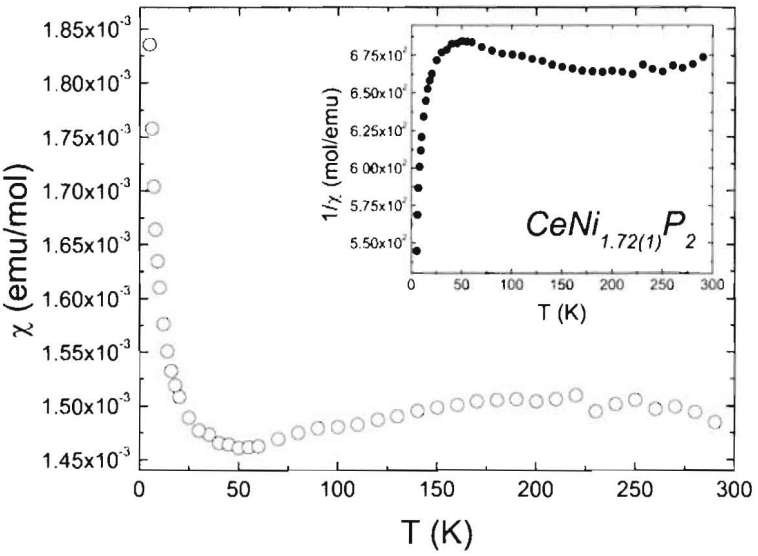


Figure 4.